Dynamical hole in ultrafast photoassociation: Analysis of the compression effect

Eliane Luc-Koenig,[1,*] Françoise Masnou-Seeuws,[1] and Ronnie Kosloff[2]
[1]*Laboratoire Aimé Cotton, CNRS, Université Paris-Sud XI, Bâtiment 505, 91405 Orsay Cedex, France*
[2]*Department of Physical Chemistry and The Fritz Haber Research Center, The Hebrew University, Jerusalem 91904, Israel*
(Received 18 July 2007; published 21 November 2007)

Photoassociation of a pair of cold atoms by excitation with a short chirped laser pulse creates a dynamical hole in the initial continuum wave function. This hole is manifested by a void in the pair wave function and a momentum kick. Photoassociation into loosely bound levels of the external well in Cs_2 $0_g^-(6S+6P_{3/2})$ is considered as a case study. After the pulse, the free evolution of the ground triplet state $a^3\Sigma_u^+$ wave packet is analyzed. Due to a negative momentum kick, motion to small distances is manifested and a compression effect is pointed out, markedly increasing the density of atom pairs at short distance. A consequence of the hole is the redistribution of the vibrational population in the $a^3\Sigma_u^+$ state, with population of the last bound level and creation of pairs of hot atoms. The physical interpretation makes use of the time dependence of the mass current and population on each channel to understand the role of the parameters of the photoassociation pulse. By varying such parameters, optimization of the compression effect in the ground-state wave packet is demonstrated. Due to an increase of the short-range probability density by more than two orders of magnitude, we predict significant gain in the photoassociation rates into deeply bound levels of the excited state by a second pulse, red-detuned relative to the first one, and conveniently delayed.

DOI: 10.1103/PhysRevA.76.053415 PACS number(s): 33.80.Ps, 32.80.Qk, 34.30.+h, 42.50.Hz

I. INTRODUCTION

One of the main outcomes of excitation of a molecular system with a short laser pulse is a "hole" in the wave function of the initial ground state [1,2]. The impulsive limit has been extended to the problem of photoassociation of ultracold atoms [3]. Due to the ultralow collision energy, this limit can be applied to a well-defined initial stationary collision state. The emphasis of that study was on optimizing the photoassociation process and the creation of stable ultracold molecules. We should complete the story and follow the dynamics of the "hole" carved out of the initial continuum wave function. We have already identified the signatures of this "hole:" (1) a void in the pair wave function of the initial state, (2) a momentum kick, initiating a motion of the hole, (3) creation of stable molecules, via population of the last bound levels of the ground electronic state, and (4) creation of pairs of hot atoms, via population of continuum levels with higher energy. The aim of the present paper is to analyze in detail the hole created in the ground-state continuum wave function, during the photoassociation pulse and after it. In Sec. II, we display results of numerical calculations on photoassociation of cesium with chirped laser pulses, showing the time evolution of the wave packet in the initial state. We identify the dynamical hole, its motion, and the compression of the initial wave function, increasing the probability density at short internuclear distances. Possible applications of this compression effect to photoassociation with a second pulse are suggested. In Sec. III we present theoretical tools for the analysis of a dynamical hole through the value of the local probability density and local momentum. In Sec. IV we make use of such tools to analyze the numerical results of Sec. II and their sensitivity to the pulse parameters (energy, duration, central frequency, sign, and value of the chirp parameter). In Sec. V we discuss how to control the formation of a dynamical hole and the compression effect, and to optimize photoassociation into vibrational levels with low v values.

II. PHENOMENOLOGICAL DESCRIPTION OF THE DYNAMICAL HOLE AND OF THE COMPRESSION EFFECT: NUMERICAL CALCULATIONS IN CASE OF CESIUM PHOTOASSOCIATION

A. The physical system

The photoassociation reaction

$$2\mathrm{Cs}(6S,F=4)+\hbar(\omega(t))\rightarrow \mathrm{Cs}_2(0_g^-(6S+6P_{3/2});v,J) \quad (1)$$

is employed as a primary example. In this reaction two ultracold cesium atoms absorb a photon red detuned from the resonance line to form a bound level (v,J) in the outer well of the excited potential curve $0_g^-(6S+6P_{3/2})$. The potential curves have been described elsewhere [3] and are displayed in Fig. 1. We shall use vibrational numbering for the double-well potential: The external well supports at least 227 levels, from $v=25$ ($v_{\mathrm{ext}}=0$) up to $v=256$, the levels $v=33,45,57,93,127$ belonging to the inner well. In the chosen example the laser pulse is a Gaussian chirped pulse of energy E_{pulse}, centered at time t_P, with a frequency

$$\omega(t)=\omega_L+\chi(t-t_P)=\frac{d}{dt}[\omega_L t+\phi(t)], \quad (2)$$

that varies linearly around the carrier frequency ω_L. In Eq. (2), we have introduced the phase $\phi(t)=\frac{1}{2}\chi(t-t_P)^2+\phi(t_P)$ of the electric field. The laser is red-detuned from the atomic D_2 line at ω_{at} by $\Delta_L=\hbar(\omega_{\mathrm{at}}-\omega_L)$, χ is the linear chirp rate in the time domain. The spectral bandwidth $\delta\omega$, defined as the full

*eliane.luc@lac.u-psud.fr

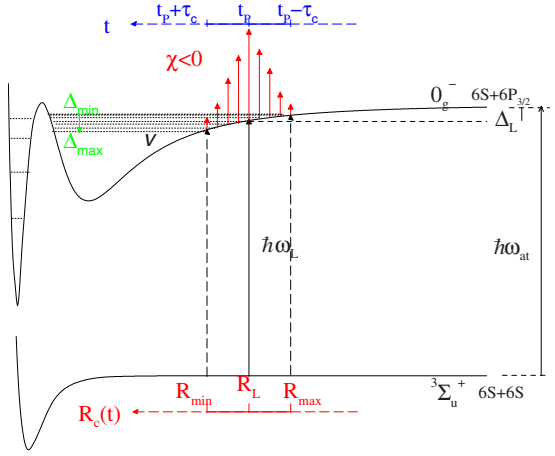

FIG. 1. (Color online) The potential curves for the lower triplet state and the double well $0_g^-(P_{3/2})$ excited state. Also indicated are the photoassociation windows in the time t (blue), energy Δ (green), and crossing distance $R_C(t)$ (red) domains in case of a pulse with negative chirp.

width at half maximum (FWHM) of the intensity profile, is related to the duration τ_L of the transform limited pulse with the same bandwidth by $\delta\omega = 4\ln 2/\tau_L \approx 14.7\ \mathrm{cm}^{-1}/\tau_L$ (in ps). The instantaneous intensity of the pulse involves a Gaussian envelope

$$I(t) = \frac{E_{\mathrm{pulse}}}{\sigma\tau_C}\sqrt{\frac{4\ln 2}{\pi}}\exp\left[-4\ln 2\left(\frac{t-t_P}{\tau_C}\right)^2\right] = I_L[f(t)]^2, \tag{3}$$

with a FWHM equal to τ_C ($\geqslant\tau_L$), the pulse duration [4]. The parameters τ_C and τ_L are related by $\chi^2\tau_C^4 = (4\ln 2)^2[(\tau_C/\tau_L)^2 - 1]$ and $[f(t_P)]^2 = \tau_L/\tau_C$. For this pulse, 98% of the energy is delivered in the time window $(t_P - \tau_C, t_P + \tau_C)$ over the illuminated area σ [3]. During this time, the instantaneous laser frequency is resonant with the excited levels with a binding energy in the range $(\Delta_L - \hbar|\chi|\tau_C, \Delta_L + \hbar|\chi|\tau_C)$, which defines a photoassociation window in the energy domain. Assuming the reflexion principle to be valid, this window can be translated into a window in the R domain, considering the outer classical turning points of the set of levels. As discussed in Ref. [5], for large enough values of the detuning, the photoassociation window in the R domain is located in a region where the nodal structure of this initial wave function is energy independent in the range defined by the thermal distribution, so that thermal averaging is straightforward. When this is not the case, numerical averaging is possible [5].

B. The two-channel coupled equations

The vibration dynamics in the ground and the excited electronic states is described by the time-dependent Schrödinger equation

$$\hat{\mathbf{H}}\Psi(\mathbf{t}) = [\hat{\mathbf{H}}_{\mathrm{mol}} + \hat{\mathbf{W}}(t)]\Psi(\mathbf{t}) = i\hbar\frac{\partial}{\partial t}\Psi(\mathbf{t}), \tag{4}$$

where $\Psi(\mathbf{t})$ is a two-component wave function describing the relative motion of the nuclei in the two channels. The molecular Hamiltonian $\hat{\mathbf{H}}_{\mathrm{mol}} = \hat{\mathbf{T}} + \hat{\mathbf{V}}_{\mathrm{el}}$ is the sum of the kinetic energy operator $\hat{\mathbf{T}}$ and electronic potential energy operator $\hat{\mathbf{V}}_{\mathrm{el}}$, with components V_{ground} and V_{exc} on the ground and excited surface respectively. The coupling term is written in the dipole approximation

$$\hat{\mathbf{W}} = -\vec{D}(\vec{R})\cdot\vec{e}_L\mathcal{E}(t),$$

$$\mathcal{E}(t) = \mathcal{E}_0 f(t)\cos[\omega_L t + \phi(t)] \tag{5}$$

involving the transition dipole moment $\vec{D}(\vec{R})$ of the dimer and the electric field defined by a polarization vector $\vec{e}_L$ assumed to be constant and by an amplitude $\mathcal{E}(t)$.

The explicit temporal dependence of the Hamiltonian $\hat{\mathbf{H}}$ is eliminated in the framework of the rotating wave approximation. In the present paper, this approximation considers the central laser frequency ω_L, multiplying the radial wave function for the nuclear motion in the ground and the excited states by $\exp(-i\omega_L t/2)$ and $\exp(+i\omega_L t/2)$, respectively, and neglecting the high-frequency component in the coupling term. This allows one to write the radial coupled equations as

$$i\hbar\frac{\partial}{\partial t}\begin{pmatrix}\Psi_g(R,t)\\ \Psi_e(R,t)\end{pmatrix} = \begin{pmatrix}\hat{\mathbf{T}} + V_g(R) & W^*\exp(i\phi)\\ W\exp(-i\phi) & \hat{\mathbf{T}} + V_e(R)\end{pmatrix}\begin{pmatrix}\Psi_g(R,t)\\ \Psi_e(R,t)\end{pmatrix}, \tag{6}$$

where the potentials are now crossing,

$$V_g(R) = V_{\mathrm{ground}} + \hbar\omega_L/2, V_e(R) = V_{\mathrm{exc}} - \hbar\omega_L/2, \tag{7}$$

and the coupling term is defined as

$$W(R,t)\exp[-i\phi(t)] = -\frac{1}{2}\vec{D}(\vec{R})\cdot\vec{e}_L\mathcal{E}_0 f(t) \times\exp\left(-\frac{i}{2}\chi(t-t_P)^2\right)\exp[-i\phi(t_P)]. \tag{8}$$

In the following calculations, the R dependence of the dipole moment is not considered, so that the amplitude of the coupling term is only time dependent and denoted by $W(t)$.

C. Results of the time-dependent calculations

Time-dependent calculations were performed by integrating Eq. (6), with a numerical method described in Refs. [3,4]. Due to the low collision energy considered, only s-wave scattering has to be accounted for. The initial state is represented by a stationary collision wave function $\Psi_g(R, t_{\mathrm{init}})$ as illustrated in the upper panel of Fig. 2, corresponding to a collision energy $E/k_B = 54\ \mu$K. For a scattering length $a \sim 300a_0$, the last node in the inner region (not considering the asymptotic sine behavior of the wave function

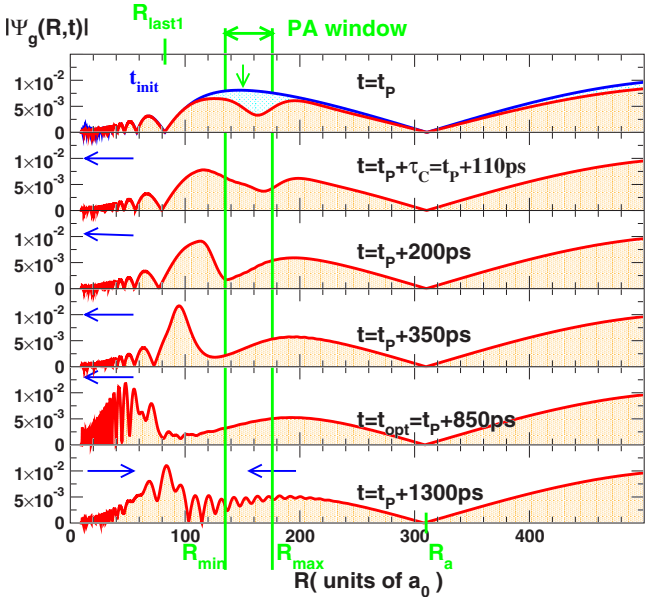

FIG. 2. (Color online) Upper panel (blue line): amplitude $A_g(R,t=t_{\text{init}})$ of the initial scattering stationary wave function for a pair of ground-state cesium atoms colliding with energy $E=k_BT$, with $T=54$ μK, and zero angular momentum, in the lack of any electromagnetic field. Note the position of the "last node" at R_a and the last but one at R_{last1}. Upper panel (red line): Amplitude $A_g(R,t=t_P)$ at the maximum of the pulse $t=t_P$: the pulse has carved out a hole in the initial wave function. This hole is indeed located in the region $[R_{\min},R_{\max}]$ of the photoassociation window, delimited by the two vertical green lines. Next panels: after the pulse, the $\Psi_g(R,t)$ wave packet moves inwards: Note the increase of the maximum value of the amplitude in the inner region. At $t-t_P$ $\sim$850 ps, the wave packet has been partly reflected by the $^3\Sigma_u^+$ inner wall located at $R\sim 10a_0$. Note that in the excited state the classical vibrational half-period for the photoassociated levels is in the $\sim$[300,600] ps range.

for a nonzero energy), hereafter referred to as "last node" is located at $R_a=310a_0$ ($\sim a$), and the last but one at $R_{\text{last1}}=82.5a_0$. In an energy range close to threshold, all nodes with $R\leqslant R_{\text{last1}}$ are energy independent. The cold atoms are illuminated by a chirped laser pulse, referred to as $\mathcal{P}_{\pm}^{122}$ in Refs. [4–6], with central detuning $\Delta_L=0.675$ cm^{-1}, duration (FWHM) $\tau_C=110$ ps, stretching factor $f_P=\tau_C/\tau_L=1.91$ associated with a transform limited pulse of duration $\tau_L=57.5$ ps and maximum intensity $I_L=120$ kW cm^{-2}. The central frequency ω_L is resonant with the level $v=153$, for which the outer turning point is located at $R_L=148.5a_0$ (corresponding to a maximum of the wave function, beween R_{last1} and R_a). For a negative chirp, the photoassociation window spans the levels $v=v_{\max}=159$ to $v_{\min}=149$, bound by 0.456 to 0.869 cm^{-1}, with a classical vibrational period T_{vib} from 1095 to 635 ps. In the R domain, the window extends from $R_{\min}=135$ to $R_{\max}=176a_0$.

The conditions for an impulsive approach are that the pulse duration is shorter than the vibrational periods [3]. At the intensity considered, the conditions for adiabatic transfer are verified, so that [3], whereas during the pulse many levels are populated, only the levels between $v_{\min}$ and $v_{\max}$ remain populated after the pulse.

D. Momentum kick on the ground $^3\Sigma_u^+$ electronic state

The generation of the depletion hole on the ground $a^3\Sigma_u^+$ electronic state can be understood by employing a phase-amplitude representation for both the ground- and the excited-state functions

$$\Psi_{g/e}(R,t)=A_{g/e}(R,t)\exp\left(\frac{iS_{g/e}(R,t)}{\hbar}\right)$$
$$=A_{g/e}(R,t)\exp\left(\frac{i\int^R p_{g/e}(R,t)dR}{\hbar}\right), \qquad (9)$$

where, within a semiclassical interpretation, $p_g(R,t)$ $[p_e(R,t)]$ is the local momentum in the ground (excited) state [7,8]. The evolution of the amplitude $A_g(R,t)$, displayed in Fig. 2, suggests the following remarks.

Before the pulse, we see in the upper panel the initial state stationary collision wave function $|\Psi_g(R,t_{\text{init}})|$ described above, and computed as a unity normalized eigenstate in a box of length $L=19\,250a_0$. In order to optimize the population transfer, we have chosen a detuning such that the photoassociation window $[135,176a_0]$ is located in the region of the "last" maximum of $|\Psi_g(R,t_{\text{init}})|$.

The laser pulse, maximum at $t=t_P$, carves out a depletion hole in the initial wave packet. The location of this hole is consistent with transfer of population to the levels $v=149$ to 159, with outer turning points from 135 to $176a_0$, located within the photoassociation window. Note that since $\int_{135}^{176}|\Psi_g(R,t_{\text{init}})|^2dR=0.0025$, only a very small fraction of the probability density in the initial state is transferred to the excited state. This very small value is due to the fact that we use a very large box. Calculations using energy-normalized initial state have been reported elsewhere [3,4], as well as determination of the absolute number of photoassociated molecules [5].

After the pulse, this hole starts moving to smaller internuclear distances, due to a negative "momentum kick" (see Refs. [1,2] and Sec. III below). Whereas the motion is taking place in a region where both V_g and $\frac{dV_g}{dR}$ are negligible, the classical velocity is quite impressive: For instance, the new maximum created on the left side of the hole and initially located at $R=110a_0$ moves to $R=90a_0$ with a velocity $\sim$4.2 m s^{-1}, two orders of magnitude larger that the classical velocity of the colliding atoms.

The motion is restricted to a localized part of the wave packet: During the time period considered here, the position of the "last" node at $R_a=314a_0$, and the wave function at distances larger than R_a, are not modified.

In contrast, we observe an increase of the probability density at distances shorter than the hole position, hereafter referred to as "compression" of the wave packet. The amplitude of the secondary maximum created on the left side of the hole increases and has grown by a factor of 2 when it reaches $R\sim 90a_0$. Therefore, at times $t-t_P\geqslant 350$ ps, (the optimal value being 850 ps), the wave packet is well adapted to photoassociation with a second pulse, red-detuned relative to the first one, populating in the excited state vibrational levels with an outer turning point around $90a_0$.

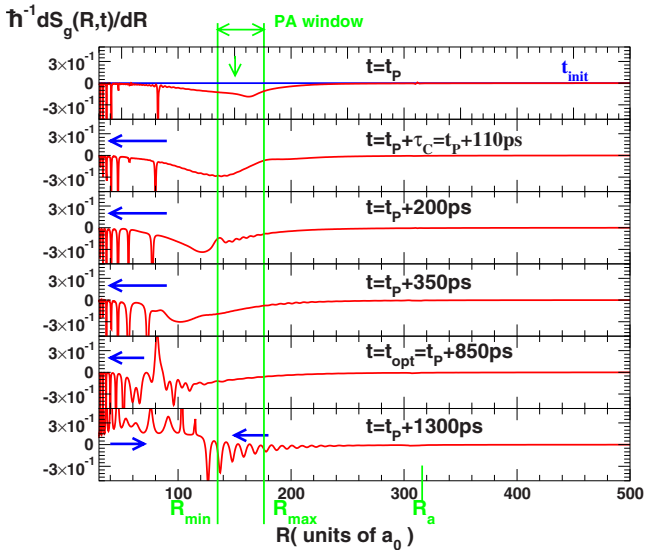

FIG. 3. (Color online) The variation of the local momentum $p_g(R,t)$ as a function of the internuclear distance. $p_g(R,t) = \partial S_g(R,t)/\partial R$, where $S_g(R,t)/\hbar$ is the phase of the wave function in the ground state [see Eq. (9) in text], for which the amplitude is displayed in Fig. 2. Just after the pulse, the value ~0.20 a.u. of the momentum created in the photoassociation window is consistent with a classical velocity of 3.6 m s^{-1}. As expected the momentum is increased in the short range region where the potential $V_g(R)$ is not negligible. The blue arrows indicate the direction of the motion.

At $t-t_P=850$ ps, the wave packet is reflected by the inner wall of the $a^3\Sigma_u^+$ potential, and starts moving outwards. Note that in the excited state the classical vibrational half-period varies from 318 for $v_{\min}$ to 548 ps for $v_{\max}$.

We may therefore conclude that after the pulse the motion of the wave packet in the ground state is governed by a timescale similar to the vibrational motion in the photoassociated levels of the excited state.

We next display in Fig. 3 several snapshots for the variation of the phase derivative $\frac{\partial S_g(R,t)}{\hbar \partial R} = p_g(R,t)/\hbar$ [see Eq. (9)], where $p_g(R,t)$ is interpreted as the local momentum [7]. Just after the pulse, a significant momentum is created in the region of the photoassociation window, where the potential and its gradient are negligible. The computed value ~0.20 a.u. corresponds to a classical velocity of 3.6 m s^{-1}, same order of magnitude as the very rough estimation of 4.2 m s^{-1} given previously. As expected, a strong momentum is observed in the short-range region ($R<30a_0$), where the potential is strongly attractive and the wave function rapidly oscillating. This will be analyzed further in Sec. III.

E. Advantage of the compression effect for photoassociation with a second pulse

To explore the possibilities offered by the compression of the wave function we have represented in Fig. 4 the time variation of the Franck-Condon overlap between $\Psi_g(R,t)$ and the stationary wave functions $\Phi_e(v)$ of the bound vibrational levels in the excited state. Almost all levels in the external well of the $0_g^-(6S+6P_{3/2})$ excited potential curve can be efficiently populated. The deepest level populated is $v=29$, $v_{\text{ext}}=4$, with a binding energy of 70 cm^{-1}, an inner turning point at $R=30a_0$, and a good Franck-Condon overlap with the $v''=42$ and 33 levels of the $a^3\Sigma_u^+$ potential, bound by 3.7 and 20.5 cm^{-1} respectively. Populating such levels can contribute efficiently to the the stabilization step.

F. Redistribution of population in the ground state: Formation of pairs of hot atoms and of halo molecules

As a result of the short pulse, the population in the ground state is redistributed. Indeed, the photoassociation reaction (1) is accompanied by a redistribution process

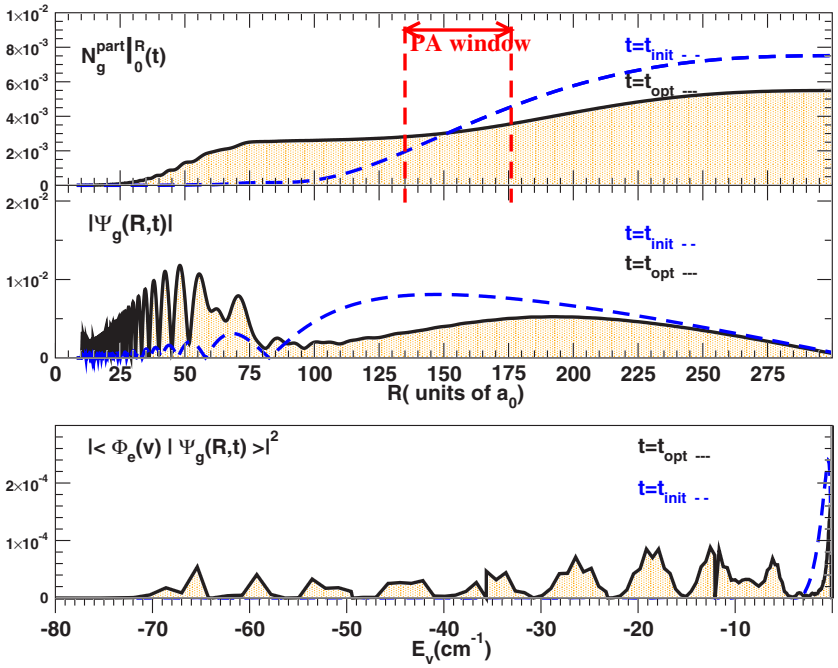

FIG. 4. (Color online) The compression effect. Intermediate panel: Wave function $|\Psi_g(R,t=t_{\text{init}})|$ of the initial collision state (blue broken line) and ground state wave packet $|\Psi_g(R,t_{\text{opt}}=t_P+850)|$ (black solid line), 850 ps after the pulse maximum, when the compression effect is maximum. Upper panel: integrated population $\int_0^R |\Psi_g(R',t)|^2 dR' = N_g^{\text{part}}|_0^R(t)$, showing the increase of the probability density at short distances from $t=t_{\text{init}}$ (blue broken line) to $t=t_{\text{opt}}$ (black solid line). Lower panel: Variation of the overlap $|\langle \Phi_e(v)|\Psi_g(R,t)\rangle|^2$ with the eigenfunctions $\Phi_e(v)$ for all the bound vibrational levels v in the $0_g^-(6S+6P_{3/2})$ excited potential curve, as a function of their energy E_v from dissociation threshold, for $t=t_{\text{init}}$ (blue broken line) and $t=t_{\text{opt}}$. Several dips visible in the overlap should be attributed to levels in the inner well ($v=33,45,57,73,93,127$).

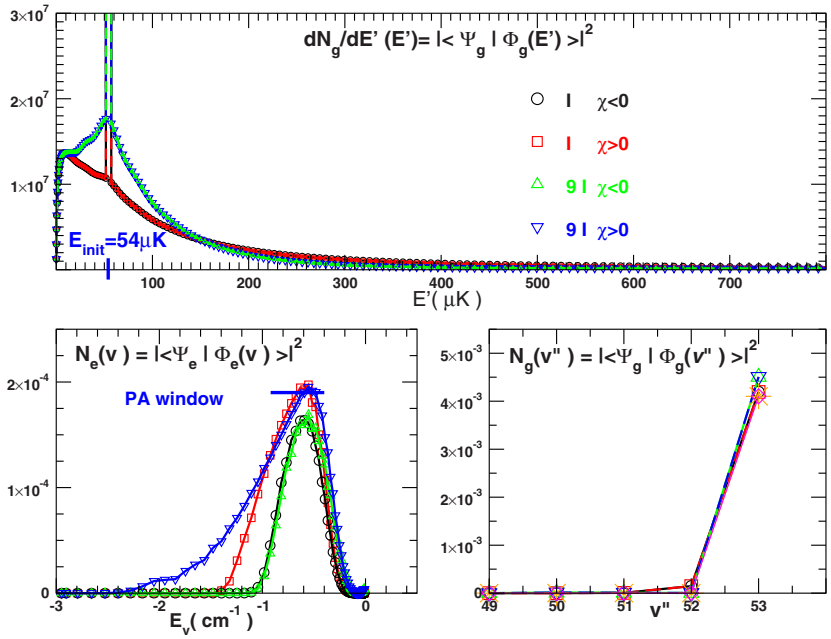

FIG. 5. (Color online) Population redistribution: Analysis of the wave packet after illuminating with the pulse P_{-}^{122}, with negative chirp (black circles), and $P_{+}^{12\bar{2}}$ (red squares). Redistribution after a similar pulse with higher intensity, changing the factor I_L in Eq. (3) to $9I_L$ (green up triangles, $\chi<0$ and blue down triangles, $\chi>0$). Upper panel: Redistribution dN_g/dE' into the continuum of the ground state, as a function of the energy E', for an initial state $E_{\text{init}}=54$ μK. The continuum levels are energy normalized. The results do not depend upon the sign of the chirp. Right lower panel: Population transfer $N_g(v'')$ to the last bound levels of the ground triplet state, as a function of the vibrational index (only the last level is populated). Left lower panel: for comparison, population transfer $N_e(v)$ to the bound levels of the excited state, as a function of their binding energy E_v.

$$2\mathrm{Cs}(6S,F=4)(E=k_BT)+\hbar[\omega(t)] \rightarrow 2\mathrm{Cs}(6S,F=4)(E'=k_BT'), \tag{10}$$

producing pairs of ground-state atoms with different energies (in particular, pairs of "hot" atoms that may leave the trap) and by an association reaction

$$2\mathrm{Cs}(6S,F=4)+\hbar[\omega(t)] \rightarrow \mathrm{Cs}_2[^3\Sigma_u^+(6S+6S);v'',J], \tag{11}$$

with formation of bound molecules in the last vibrational levels of the $a^3\Sigma_u^+$ potential.

The redistribution into the stationary levels of the ground state potential is analyzed in Fig. 5 by projecting the free-evolving wave packet $\Psi_g(R,t)$ after the pulse on eigenstates of the $[\hat{\mathbf{T}}+V_g(R)]$ Hamiltonian. We consider both energy-normalized continuum levels $\Phi_g(E')$ with positive energy $(E'=k_BT')$ and bound levels $\Phi_g(v'')$ with negative energy. The population $N_g(v'')$ of the bound levels is determined, as well as the density of population $dN_g(E')/dE'$ for energy-normalized continuum levels. Since the calculations are considering an unity-normalized initial state, the initial distribution of population is very narrow $[dN_g(E')/dE' \sim 1.1 \times 10^{11}\delta(E_{\text{init}}-E')]$. We have studied the sensitivity to the pulse parameters: The redistribution is independent of the sign of the chirp; in contrast, when the maximum intensity of the pulse is increased by augmenting I_L [see Eq. (3)], the width of the redistribution of collision energies is clearly reduced. Note that the area below the curve is roughly conserved, changing from 0.0097 to 0.011 when the intensity increases by a factor of 9.

Population is also transferred efficiently to bound levels of the ground triplet state, primarily to the last bound level $v''=53$, creating a halo molecule. This mechanism is similar to the population transfer to the last bound level achieved by sweeping an optical Feshbach resonance. The population does not depend upon the sign of the chirp. The number of ground-state halo molecules (0.004) is of the same order of magnitude as the number of photoassociated molecules (0.002), as can be seen by comparing the left and right lower panels of Fig. 5, in accordance with Ref. [3]. It should be noticed that the population of the photoassociated molecules is spread over more than 30 vibrational levels.

While a change of the sign of the chirp is not modifying the population of the last bound level and the redistribution into continuum levels, it has a strong influence on the photoassociation efficiency (see left panel of Fig. 5). For $\chi<0$, the levels populated in $0_g^-(6S+6P_{3/2})$ are within the photoassociation window, and the population depends weakly upon I_L. For $\chi>0$, the distribution extends to levels outside the photoassociation window, and this effect increases with intensity. As discussed in Refs. [10,11], for $\chi<0$ the instantaneous frequency "follows" the motion of the wave packet, so that the population is brought back to the ground state and up again. This phenomenon is labeled "multiple interaction" in Ref. [11]. For $\chi>0$, this recycling effect is much weaker: Once a level is populated, the instantaneous frequency is no longer resonant with its energy, and the population remains in this photoassociated level. This recycling effect will be discussed further in the following sections.

III. THE PARTIALLY INTEGRATED POPULATION AND MASS CURRENT AS A TOOL FOR INTERPRETATION

A. Local current density, local momentum, and local probability density

In order to get a better insight into the hole dynamics one has to follow both the population depletion as well as the local value of the momentum induced by the laser field [1,2]. For the problem of photoassociation, a global quantum analysis of the total changes in population and in momentum due to the pulse has been discussed recently [9]. This formal-

ism, based on Heisenberg equations, is adapted to the implementation of local control theory. In the present work we use a local framework closer in spirit to the phase-amplitude separation [see Eq. (9)], and based on the change in time of the radial component of the probability current density [7,8], hereafter, named local current density. The analysis is carried out for both the ground- and excited-state components of the wave function as defined in Eq. (6),

$$j_{g/e}(R,t) = \frac{\hbar}{2mi}\left[\Psi^*_{g/e}(R,t)\frac{\partial\Psi_{g/e}(R,t)}{\partial R} - \frac{\partial\Psi^*_{g/e}(R,t)}{\partial R}\Psi_{g/e}(R,t)\right], \quad (12)$$

where m is the reduced mass. The local momentum, defined in Eq. (9), and called "state momentum" in Ref. [10], is related to the local current density

$$p_{g/e}(R,t) = \frac{\partial S_{g/e}(R,t)}{\partial R} = \frac{mj_{g/e}(R,t)}{|\Psi_{g/e}(R,t)|^2} = \frac{mj_{g/e}(R,t)}{|A_{g/e}(R,t)|^2}, \quad (13)$$

where the phase and amplitude have been defined in Eq. (9).

The formulation is related to the classical limit of Bohmian dynamics [12], where one considers on each channel the motion of a fluid of noninteracting particles with mass m, local probability density $|A_{g/e}(R,t)|^2$, probability current density $j_{g/e}(R,t)$, driven by a time-dependent force $F^B_{g/e}(R,t) = \frac{dp_{g/e}}{dt} = \left(\frac{\partial}{\partial t} + \frac{\partial}{\partial R}\frac{\partial R}{\partial t}\right)p_{g/e}(R,t)$. This aspect will be discussed in a forthcoming paper [13].

The time derivative of the two quantities $mj_g(R,t)$ and $mj_e(R,t)$ reads

$$m\frac{\partial j_g(R,t)}{\partial t} = F_g(R)|A_g(R,t)|^2 + \mathcal{K}_g(R,t) + \mathcal{L}(R,t), \quad (14)$$

$$m\frac{\partial j_e(R,t)}{\partial t} = F_e(R)|A_e(R,t)|^2 + \mathcal{K}_e(R,t) - \mathcal{L}(R,t). \quad (15)$$

We have defined the following three terms:

(1) The classical force for each potential

$$F_{g/e}(R) = -\frac{dV_{g/e}}{dR}, \quad (16)$$

so that the first term in Eqs. (14) and (15) depends both upon the classical force and the local probability density $A^2_{g/e}(R,t)$ in the channel considered, defining a time-dependent density of force $F_{g/e}(R)A^2_{g/e}(R,t)$.

(2) A kinetic term due to the non-Hermiticity of the local kinetic energy operator

$$\mathcal{K}_{g/e}(R,t) = \frac{\partial}{\partial R}\left[\frac{\hbar^2}{4m^2}\left(\Psi^*_{g/e}(R,t)\frac{\partial^2\Psi_{g/e}(R,t)}{\partial R^2} + \frac{\partial^2\Psi^*_{g/e}(R,t)}{\partial R^2}\Psi_{g/e}(R,t)\right) - 2\left(\frac{\partial\Psi^*_{g/e}(R,t)}{\partial R}\frac{\partial\Psi_{g/e}(R,t)}{\partial R}\right)\right]. \quad (17)$$

This complicated term, arising from the fact that the time variation of $j(R,t)$ results both from the time variation of the local momentum $p(R,t)$ and of the local probability density $|A(R,t)|^2$ will be discussed further in a forthcoming paper [13].

(3) A third term due to the coupling of the two channels by the laser field, which cancels when the laser is off, and has an opposite sign in the ground and in the excited state

$$\mathcal{L}(R,t) = \mathrm{Re}\left[\Psi^*_e(R,t)\frac{\partial}{\partial R}\{W(t)\exp[-i\phi(t)]\Psi_g(R,t)\}\right] - \mathrm{Re}\left[W^*(t)\exp[i\phi(t)]\Psi^*_g(R,t)\frac{\partial\Psi_e(R,t)}{\partial R}\right]. \quad (18)$$

It depends upon the coupling (amplitude W, phase ϕ, and therefore sign of the chirp) and also upon the phase difference between the wave packets in the ground and excited states. Introducing the momentum operator $\hat{\mathbf{P}} = -i\hbar\partial/\partial R$, one may rewrite

$$\mathcal{L}(R,t) = -\frac{1}{\hbar}[\mathrm{Im}(\Psi^*_e(R,t)\hat{\mathbf{P}}\{W(t)\exp[-i\phi(t)]\Psi_g(R,t)\}) - \mathrm{Im}(\Psi^*_g(R,t)\{W^*(t)\exp[+i\phi(t)]\hat{\mathbf{P}}\Psi_e(R,t)\})]. \quad (19)$$

Note that the density of force $\mathcal{L}(R,t)$ is zero if the laser field is zero, of course, but also when the local probability density either in the ground or the excited state is zero.

Another set of equations, complementary to Eqs. (14) and (15) describes the time variation of the local probability density

$$m\frac{\partial A_g(R,t)^2}{\partial t} = -\frac{\partial j_g(R,t)}{\partial R} - \frac{2}{\hbar}\mathrm{Im}[\Psi^*_e(R,t)W(t) \times \exp[-i\phi(t)]\Psi_g(R,t)], \quad (20)$$

$$m\frac{\partial A_e(R,t)^2}{\partial t} = -\frac{\partial j_e(R,t)}{\partial R} + \frac{2}{\hbar}\mathrm{Im}[\Psi^*_e(R,t)W(t) \times \exp[-i\phi(t)]\Psi_g(R,t)]. \quad (21)$$

When the laser is off, Eqs. (20) and (21) are the relations of flux conservation on each channel. During the pulse, exchange of population between the two channels is taking place due to the last term in the right member.

B. Integrated and partially integrated values

With the concept of the photoassociation window in mind we can differentiate between the local and global influence of the pulse. For the global effect, we have considered the R-integrated values over the total box of length L. We define from the local current densities $j_{g/e}(R,t)$, local probability densities $|A_{g/e}(R,t)|^2$, and from their time derivatives, the integrated functions

$$mI_{g/e}(t) = \int_0^L mj_{g/e}(R,t)dR$$

$$= \int_0^L \Psi^*_{g/e}(R,t)p_{g/e}(R,t)\Psi_{g/e}(R,t)dR, \quad (22)$$

$$m\frac{dI_{g/e}(t)}{dt} = m\int_0^L \frac{\partial j_{g/e}(R,t)}{\partial t}dR, \quad (23)$$

$$N_{g/e}(t) = \int_0^L |A_{g/e}(R,t)|^2 dR, \quad (24)$$

$$\frac{dN_{g/e}(t)}{dt} = \int_0^L \frac{\partial |A_{g/e}(R,t)|^2}{\partial t}dR. \quad (25)$$

$mI_{g/e}(t)$ is the mass current and $N_{g/e}(t)$ is the number of particles. In Ref. [9], similar quantities are obtained directly from the Heisenberg equations and related to the "average momentum" and "population" on each channel. For the chosen integration domain $(0,L)$, the quantities corresponding to the integrated value of $\mathcal{K}_{g/e}(R,t)$ in Eqs. (14) and (15) disappear: The Hermiticity of the kinetic energy operator results into $\int_0^L \mathcal{K}_{g/e}(R,t)dR=0$ and one obtains

$$m\frac{dI_{g/e}(t)}{dt} = \int_0^L F_{g/e}(R)A^2_{g/e}(R,t)dR \pm \int_0^L \mathcal{L}(R,t)dR, \quad (26)$$

where the last term in the right-hand side describes the momentum exchange between the two channels due to laser coupling, as discussed in Ref. [9]. Therefore,

$$m\frac{d[I_g(R,t)+I_e(R,t)]}{dt} = \int_0^L [F_g(R)|A_g(R,t)|^2 + F_e(R) \times |A_e(R,t)|^2]dR, \quad (27)$$

where the term due to laser coupling has indeed disappeared. Before the pulse, $mI_g(t)=0$, since the initial state is a stationary state. The "momentum kick" in the ground state, once the laser is off, is characterized by a nonzero mass current $mI_g(t>t_P+\tau_C)$.

However, for the analysis of the photoassociation effect, where the process is taking place within a photoassociation window, a local view is consistent with partially integrated values. We have therefore considered also the time-dependent quantities $I^{\text{part}}_{g/e}(t)|^{R_2}_{R_1}$ and $N^{\text{part}}_{g/e}(t)|^{R_2}_{R_1}$ defined as integrals

$$mI^{\text{part}}_{g/e}(t)|^{R_2}_{R_1} = m\int_{R_1}^{R_2} j_{g/e}(R,t)dR, \quad (28)$$

$$N^{\text{part}}_{g/e}(t)|^{R_2}_{R_1} = \int_{R_1}^{R_2} A^2_{g/e}(R,t)dR, \quad (29)$$

taken on a limited range of internuclear distances (R_1,R_2), that could be the photoassociation window $(R_{\min},R_{\max})$. In the general case, the influence of the kinetic term $\int_{R_1}^{R_2}\mathcal{K}_{g/e}(R,t)dR$ will manifest itself. This will be discussed in detail in a forthcoming paper [13].

In the present work the limited range was chosen as $(0,R_a)$, so that $\int_0^{R_a}\mathcal{K}_{g/e}(R,t)dR$ is negligible since $\Psi_{g/e}(R_a,t)=0$. R_a is the position of the "last" node, which stays fixed during and after the $\mathcal{P}^{122}_-$ photoassociation pulse (see Fig. 2), as discussed above in Sec. II C. The justification for such a choice is that at large distance, where the potentials are negligible and the dipole moment $D(R)$ constant, the wave function in the excited state merely reflects the initial wave function [4,5]. Writing

$$\Psi_{g/e}(R,t) \sim \alpha_{g/e}(t)\Psi_g(R,t_{\text{init}}), \quad R > R_a,$$

where $\alpha_{g/e}(t)$ is a complex number, such that $\alpha_e(t \gg \tau_C)=0$, it is clear that there is no R dependence of the phase $S_{g/e}(R,t)$. Therefore, under the conditions where adiabatic population transfer takes place within a photoassociation window, for large distances outside this window, the momentum kick is zero. The analysis of the photoassociation dynamics can then safely be restricted to the $R<R_a$ range.

In the following we shall simplify the notations by writing

$$I^{\text{part}}_{g/e}(t) = I^{\text{part}}_{g/e}(t)|^{R_a}_0, \quad (30)$$

$$N^{\text{part}}_{g/e}(t) = N^{\text{part}}_{g/e}(t)|^{R_a}_0. \quad (31)$$

We shall also use a "partially integrated" time-dependent force

$$F^{\text{part}}_{g/e}(t) = \int_0^{R_a} F_{g/e}(R)A^2_{g/e}(R,t)dR. \quad (32)$$

The average value of the momentum gained during the pulse by the inner part of the ground-(excited-) state wave packet can be evaluated from the mass current and the partial population by

$$\langle P^{\text{part}}_{g/e}(t)\rangle = \frac{mI^{\text{part}}_{g/e}(t)}{N^{\text{part}}_{g/e}(t)}. \quad (33)$$

IV. ANALYSIS OF THE RESULTS

A. Analysis of the results for the pulse $\mathcal{P}^{122}_-$

A comparison of the time variation of $mI_{g/e}(t)$, $N_{g/e}(t)$, and their time derivatives, as well as of the partially integrated quantities $mI^{\text{part}}_{g/e}(t)$, $N^{\text{part}}_{g/e}(t)$ is reported in Fig. 6, leading to the following remarks.

(1) During the time window $t_P-\tau_C<t<t_P+\tau_C$, there is a large population exchange between the two channels: In the lower figure of the left panel $\frac{dN_e(t)}{dt}=-\frac{dN_g(t)}{dt}$ displays a variation roughly identical to the shape of the pulse, apart from small oscillations. The range of distances $R>R_a=314a_0$ contributes very much to this population transfer, and we see

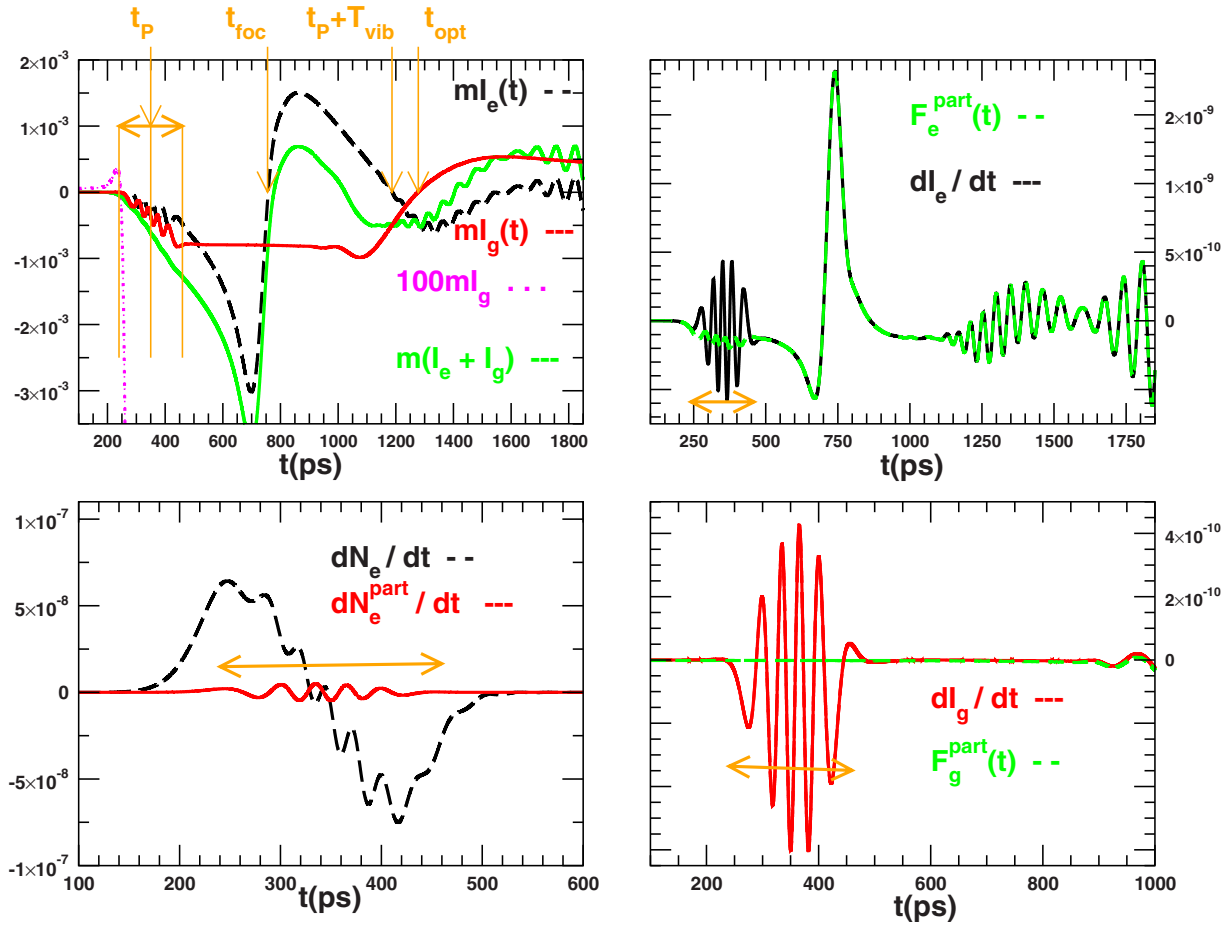

FIG. 6. (Color online) Photoassociation with the pulse $\mathcal{P}_{-}^{122}$, with negative chirp and small detuning, maximum at $t=t_P=350$ ps: the time window $[t_P-\tau_C,t_P+\tau_C]$ is indicated by the horizontal arrow. Left column: In the upper figure the mass currents $mI_g(R,t)$ (red solid line) in the ground state and $mI_e(R,t)$ (black broken line) in the excited state, and their sum (green solid line), as a function of time [see Eqs. (23) and (27) in text] are represented. Note the Rabi oscillations during the pulse. A small current in the ground state at the beginning of the pulse is drawn (dotted line) as enhanced by a factor of 100. In the lower figure, the time variation of the population is displayed: the calculations have been done by summing over the full range of distances (black broken line) and by restricting to $R<R_a=314a_0$ (red solid line). It is clear that a large amount of population is transferred at large distances during the pulse. In the right column, the time variation of $mdI_{g/e}(t)/dt$ [see Eq. (26) in text] in the excited (upper figure, black solid line) and in the ground state (lower figure, red solid line) is compared to the "classical" forces (broken green line) $F_{g/e}^{\text{part}}$ [see Eq. (32) in text], showing a strong enhancement during the pulse. Note that the classical force is negligible in the ground state but not in the excited state. After the pulse, the time variation of the mass currents is entirely determined by the classical forces. The wave packet in the excited state is focalized at the inner turning point at $t=t_{\text{foc}}$, and reaches the outer turning point after one vibrational period T_{vib}.

that the variation of the partial population $\frac{dN_e^{\text{part}}(t)}{dt}$ is much smaller than $\frac{dN_e(t)}{dt}$.

(2) Just after the pulse, however, the wave packet in the excited state is localized in the photoassociation window, as discussed previously [3,4].

(3) There is no momentum exchange between the two channels at large distances, and we find $I_{g/e}(t)\sim I_{g/e}^{\text{part}}(t)$. Indeed, in the region $R>R_a$ the phase is R independent on both channels $\left(\frac{\partial S_{g,e}(R,t)}{\partial R}=0\right)$, so that $I_{g/e}^{\text{part}}(t)|_{R_a}^{\infty}=0$.

(4) At the very beginning of the pulse, for times $t<t_P-\tau_C$, when, due to low laser intensity the (small) population transfer is not adiabatic, the ground-state wave packet gains a positive momentum. The total mass current $m(I_g+I_e)$ is conserved, the contribution of the classical force being negligible [1].

(5) During the time window $[t_P-\tau_C,t_P+\tau_C]$, there is an exchange of momentum between the ground and the excited state. The two mass currents mI_g and mI_e are oscillating with opposite phase, in agreement with Eq. (26).

(6) The sum of the mass current on the two channels is not oscillating, in agreement with Eq. (27). Due to the large acceleration in the excited potential (see the upper figure in the right pannel), this sum current is smoothly decreasing.

(7) For $t_P-\tau_C<t<t_P$ the two channels are equally sharing the classical acceleration due to the R^{-3} asymptotic behavior of the $0_g^-(6S+6P_{3/2})$ potential, so that $I_g(t)$ and $I_e(t)$ are oscillating with opposite phase below and above their mean value.

(8) For $t_P<t<t_P+\tau_C$ the mass current gain in the ground state becomes larger than in the excited state: The acceleration is no longer equally shared between the two channels.

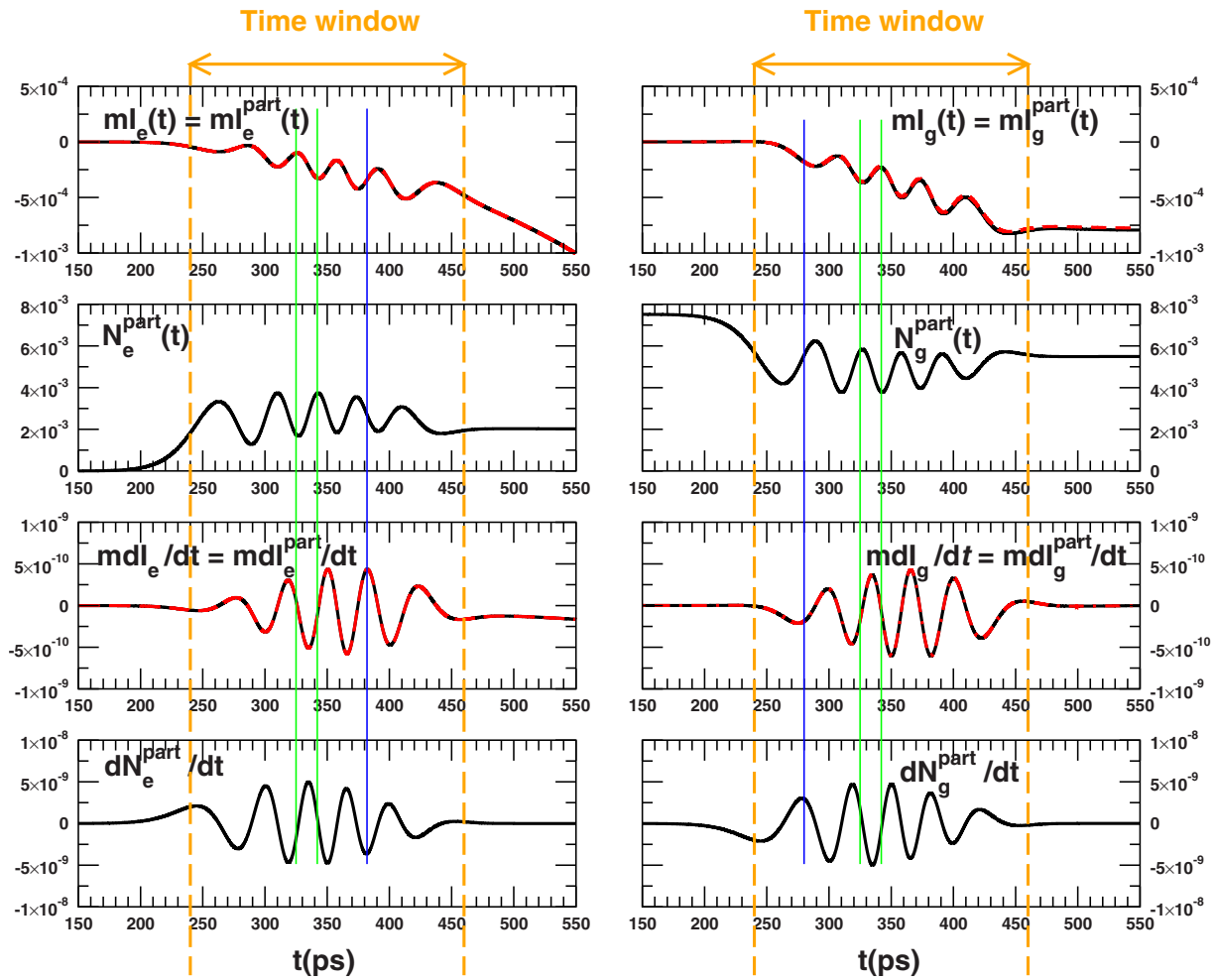

FIG. 7. (Color online) Evidence for a momentum kick in the ground state. The laser pulse is $\mathcal{P}_{-}^{122}$, maximum at time t_P=350 ps. Top figures: Time variation of the mass current $mI_e(t)=mI_e^{\mathrm{part}}(t)$ (left) and $mI_g(t)=mI_g^{\mathrm{part}}(t)$ (right) on the two channels. Middle pannel: Time variation of the partial populations $N_g^{\mathrm{part}}(t)$ and $N_e^{\mathrm{part}}(t)$ in the range $[0,R_a=314a_0]$ of internuclear distances. Lower pannels: Time derivatives of the same quantities. The vertical lines are drawn to emphasize the phase of the Rabi oscillations for each quantity. The pulse is present during the time window [240,460] ps. After the pulse, although for the ground state wave packet the classical force is negligible $[dI_g(t)/dt=0]$, the mass current $mI_g(t)$ is negative and constant, manifesting the momentum kick.

(9) During the pulse, the variation of the time derivatives $m\frac{dI_{g/e}(t)}{dt}$ in Eq. (26) is dominated by the term $\int_0^{R_a}\mathcal{L}(R,t)dR$. The laser-induced forces arising from this term are much larger than the classical forces involved in $\int_0^{R_a}F_{g/e}(R)A_{g/e}^2(R,t)dR$.

(10) After the pulse, the inner part of the wave packet in the excited state is accelerated towards short distances, due to the classical force. The pulse $\mathcal{P}_{-}^{122}$ has been optimized for focussing this vibrational wave packet half a vibrational period after the pulse maximum [3]: For the levels considered, 318 ps$\leqslant T_{\mathrm{vib}}(v)/2\leqslant$550 ps. The reflexion on the inner wall occurs during a very short time interval, in the range $t_P-\tau_C+T_{\mathrm{vib}}(v_{\max})/2$, $t_P+\tau_C+T_{\mathrm{vib}}(v_{\min})/2$, i.e., (778,790) ps. Defining $t=t_{\mathrm{foc}}\sim$784 ps, we may see in Fig. 6 a sudden change of the sign of I_e at $t=t_{\mathrm{foc}}$.

(11) In contrast, as can be seen in the lower figure of the right pannel, the classical force is zero in the ground state. After the pulse, I_g remains constant during a long time interval of $\sim$600 ps. Since the population remains constant, this corresponds to a constant velocity. The part of the wave packet that is located at $R<R_a$ is moving to short distances with constant velocity for a duration of $\sim$600 ps, in a region where there is no potential gradient. We then see the evidence for a negative momentum kick due to the laser pulse.

(12) For $t-t_P>\tau_C+600$ ps, the wave packet in the ground state reaches distances where the $a^3\Sigma_u^+$ potential is no longer negligible: it is accelerated at $t>1000$ ps, then partly reflected by the inner wall at $t\sim$1100 ps. At $t=t_{\mathrm{opt}}$=1300 ps ($t-t_P$=950 ps), the mean velocity vanishes, which corresponds to the optimal time for reexcitation by a second pulse (see Fig. 4).

The oscillations which appear during the pulse in the time variation of the populations or of the mass currents are analyzed in more detail in Fig. 7. These Rabi oscillations are induced by the laser field: Indeed, for the $\mathcal{P}_{-}^{122}$ pulse, the

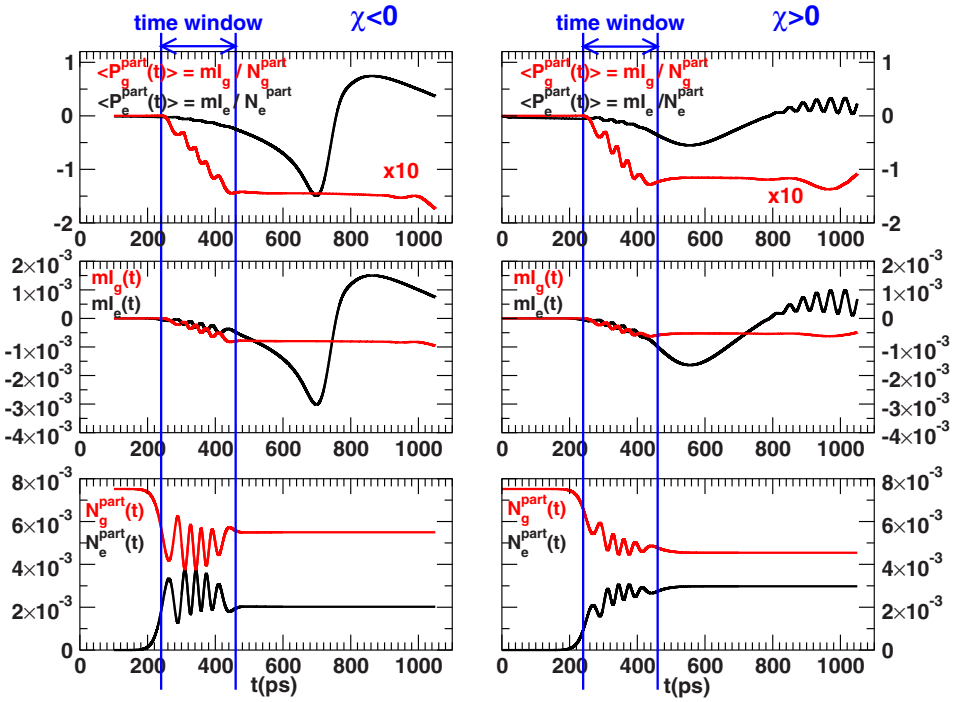

FIG. 8. (Color online) Average momentum and influence of the sign of the chirp. Left pannel: Photoassociation with the pulse $\mathcal{P}_{-}^{122}$, with negative chirp. Upper figure: Average value of the momentum $\langle P_g^{\mathrm{part}}(t)\rangle$ (red line) for the ground state and $\langle P_e^{\mathrm{part}}(t)\rangle$ for the excited state (black line), as defined in Eq. (33). Middle figure: The mass current $mI_g(t)$ (red line) and $mI_e(t)$ (black line). Lower figure: Population in the ground state $N_g^{\mathrm{part}}(t)$ in the region $R<314a_0$ (red line), and in the excited state $[N_e^{\mathrm{part}}(t)$, black line]. Right pannel: Same quantities for photoassociation with the pulse $\mathcal{P}_{+}^{122}$, with positive chirp.

Rabi frequency at resonance, evaluated as $\Omega(t)=\frac{1}{\hbar}|W(t)|$, satisfies

$$\int_{t_P-\tau_C}^{t_P+\tau_C}\Omega(t)dt \sim 5.3\Pi,$$

which is the same order of magnitude as the number of oscillations visible in the figure.

The Π phase difference between the oscillations of the populations N_g and N_e results from the conservation of population. The Π phase difference between the oscillations of the mass current mI_g and mI_e results from the $\pm\int_0^L \mathcal{L}(R,t)dR$ laser coupling term in Eq. (26).

In each channel, the Π phase difference between the time variation of I and N points out that, both in Eqs. (14) and (15) and in Eqs. (20) and (21), the laser coupling term dominates, so that the change in the mass current is mainly caused by the change of population. In other words, it is the exchange of population between the two channels that induces the momentum kick in the ground state, since the population transferred back to the ground-state brings back a negative momentum. It is the Rabi cycling phenomenon, and the efficiency in recycling population that seems the key factor in inducing a motion of the ground-state wave packet towards short distances.

The average value $\langle P_g^{\mathrm{part}}(t)\rangle$ of the momentum gained during the pulse by the inner part of the ground-state wave packet, evaluated through Eq. (33), as well as $\langle P_e^{\mathrm{part}}(t)\rangle$, are represented in the left upper pannel of Fig. 8. The Rabi oscillations observed in the time-variation of $mI_g^{\mathrm{part}}(t)$ and $N_g^{\mathrm{part}}(t)$ being of opposite phase, they disappear almost completely in $\langle P_g^{\mathrm{part}}(t)\rangle$, which proves again that the oscillations in $mI_g^{\mathrm{part}}(t)$ are almost entirely due to the population. The mean negative velocity gained by the ground state wave packet is ~ 2.7 m s^{-1}, in agreement with the previously estimated value.

B. Sensitivity to the sign of the chirp parameter and to the intensity

The sensitivity to the sign of the chirp is illustrated in the right pannel of Fig. 8, where are reported calculations done for the photoassociation pulse $\mathcal{P}_{+}^{122}$ similar to the previous one but for $\chi>0$. The maximum population transferred to the excited state during the pulse is much smaller than for a negative chirp, the amplitude of the oscillations being also smaller. However, after the pulse, the population remaining in the excited state is 0.003, larger by a factor 1.5 than for $\chi<0$. Looking at the mean value of the population, we see that recycling occurs for the pulse $\mathcal{P}_{-}^{122}$ whereas for a positive chirp a regular increase of the population is observed. This recycling effect can be attributed to the multiple interactions [10,11] occurring for a negative chirp, when the motion of the two wave packets is "following" the pulse, and not for a positive chirp.

After the $\mathcal{P}_{+}^{122}$ pulse, the wave packet in the excited state is spreading, since there is no focussing effect: The reflexion on the inner wall takes place during a longer time interval than for $\chi<0$, from $t_P-\tau_C+\frac{1}{2}T_{\mathrm{vib}}(v_{\mathrm{min}})=560$ ps to $t_P+\tau_C+\frac{1}{2}T_{\mathrm{vib}}(v_{\mathrm{max}})=1000$ ps. Starting from $t=800$ ps, the large spread of the wave packet gives rise to interferences between components moving in the opposite direction.

The mean momentum gained by the inner part of the wave packet after the $\mathcal{P}_{+}^{122}$ pulse corresponds to a mean velocity of 2.1 m s^{-1}, a factor 1.3 smaller than in the case of the negative chirp. It seems that the momentum kick is favored by important Rabi oscillations and a smaller photoassociation efficiency.

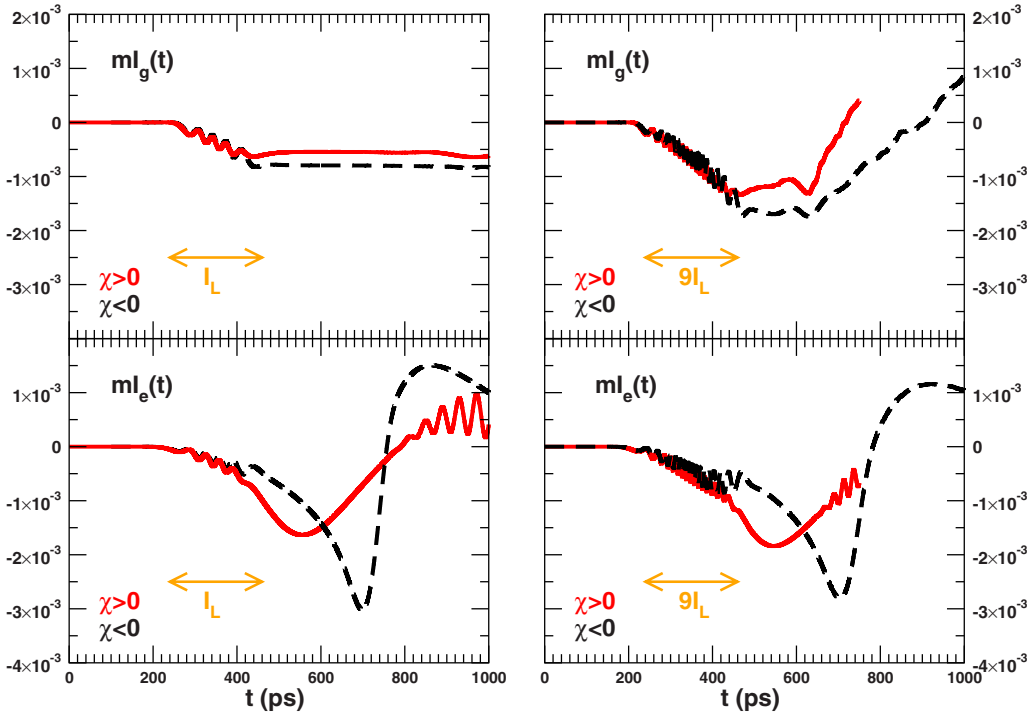

FIG. 9. (Color online) Effect of the sign of the chirp and of the intensity of the photoassociation pulse. Time variation of the mass currents mI_g in the ground state (upper figures) and mI_e in the excited state (lower figures). Left column, calculations with the pulses $\mathcal{P}_-^{122}$ (black broken lines), $\mathcal{P}_+^{122}$ (red solid lines) as in Fig. 8. The time windows are indicated by horizontal arrows. Right column: Same calculations, increasing the coupling in Eqs. (6) by a factor of 3, or the intensity I_L in Eq. (3) by a factor of 9 and considering negative (black broken lines) and positive (red solid lines) chirp. The increase of the momentum kick in the ground state is clearly manifested. The reflexion on the inner wall becomes visible in the time window considered.

The effect of the laser intensity is discussed in Fig. 9. When the intensity is increased by a factor of 9, the number of Rabi oscillations during the pulse increases by a factor of 3 as expected. The transfer of population after the pulse $N_e^{\text{part}}(t>t_P+\tau_C)$ increases by 20% (from 0.002 to 0.0024) for $\chi<0$ and by 30% (from 0.003 to 0.0038) for $\chi>0$.

When considering the larger intensity and a negative chirp, the momentum kick in the inner part of the ground-state wave packet is increased by a factor of ~2. The inner part of the wave packet moves to short distances with a mean velocity of ~6 ms^{-1} (compared to 2.7 previously): the reflexion on the inner wall of the $a^3\Sigma_u^+$ potential, with $I_g(t)=0$, occurs ~400 ps after the pulse maximum, to be compared with the value 950 ps in the previous case. For positive chirp, the momentum kick in the ground state is now very close to the values obtained for $\chi<0$. However, since in the latter case the population $N_g^{\text{part}}(t>t_P+\tau_C)$ is larger by a factor of 1.5 than for $\chi>0$, a more important compression effect is to be expected for negative chirp.

The previous analysis shows that the relative gain in momentum on the two channels can be modified by changing the parameters of the pulse. The best way to optimize the latter is an open problem.

C. Local and nonlocal effects

During the pulse, the variation of the local current density on each channel, as described in Eqs. (14) and (15), as well as the local probability density [see Eqs. (20) and (21)] depend upon coupling terms involving both the laser coupling $W(t)\exp[-i\phi(t)]$ and either $\Psi_e^*(R,t)\frac{\partial\Psi_g(R,t)}{\partial R}$ or $\Psi_e^*(R,t)\Psi_g(R,t)$. The important quantity is then the phase difference

$$\frac{S_g(R,t)}{\hbar}-\frac{S_e(R,t)}{\hbar}-\phi(t) \tag{34}$$

which depends both upon t and R. In our problem, the initial wave function $\Psi_g(R,t)$ is delocalized, and extends over the full range of internuclear distances. Therefore during the pulse the excited wave packet $\Psi_e(R,t)$ will also be delocalized. However, for very large distances, neither $S_g(R,t)$ nor $S_e(R,t)$ present a R dependence. In Fig. 10, the R variation of $\frac{\partial S_{g/e}(R,t)}{\hbar\partial R}$ is represented for various times in the vicinity of the pulse maximum. For distances up to $250a_0$, very rapid changes of the phase occur, and a very complicated R dependence is manifested. This suggests that the choice of R-integrated physical quantities, as used in Refs. [9,10], to optimize the pulse, may not be a very efficient procedure once the delocalized character of the initial wave function is introduced in the model.

In the "single pulse Raman-like walk scheme" of Ref. [10], the initial state is a localized Gaussian wave packet, and the control parameter is the laser instantaneous frequency, designed to match the collision dynamics at distances $R<40a_0$, by inducing multiple coherent upward and down-

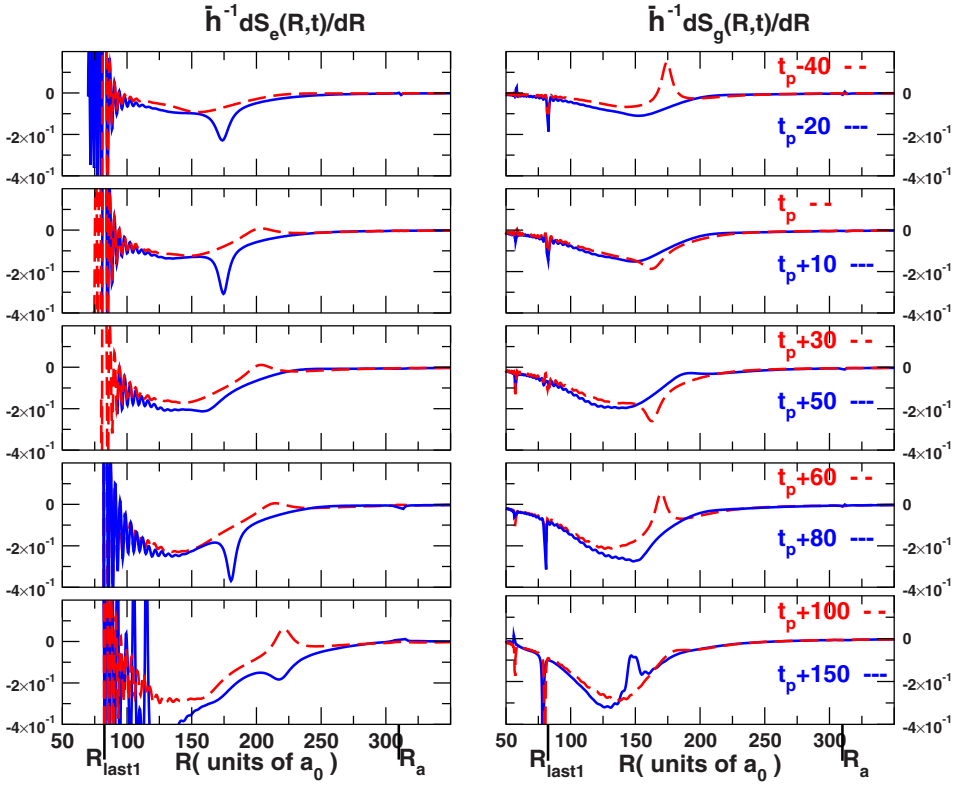

FIG. 10. (Color online) Snapshots, at various times during the pulse of the variation of the local momentum $\frac{\partial S_{g/e}(R,t)}{\hbar \partial R}$, see Eq. (9), as a function of the internuclear distance R. This figure is giving more detailed information than Fig. 3: The strong variation of the phase, as a function both of the distance R and of the time t (t_P corresponding to the maximum intensity) is demonstrated. The position R_a of the "last node" in the initial wave function, and R_{last1} of the previous one are indicated by arrows.

ward transitions. It seems that for this "matched spectrum pulse," a lot of population is redistributed into continuum levels of the ground state, creating pairs of hot atoms rather than the target bound levels in the ground state. In Ref. [9], the global phase of matrix elements such as $\langle \Psi_e(R,t)|D(R)|\Psi_g(R,t)\rangle$ and $\left\langle \Psi_e(R,t)\left|D(R)\right|\frac{\partial \Psi_g(R,t)}{\partial R}\right\rangle$ is the control parameter. The phase of the field is then following the variation in the phase of the expectation value to be controlled. It then seems that for a pulse duration larger than 1 ps, the efficiency of the control is dropping.

The choice of a spatially global operator such as the total population or the total momentum can overlook the finer details of controlling a localized quantity. This is equivalent to the quantities R integrated over the total box in the present paper, which lose a large part of the phase information. Therefore, the partially integrated quantities (29) and (31) are a better choice, enabling a better optimization of the compression effect. In the next paper [13] the current approach will be linked to a different set of spatially semilocal operators. However, from the present analysis of the partially integrated quantities, we have drawn a few conclusions that might help to optimize the compression effect.

V. CONTROL OF THE COMPRESSION EFFECT

From the discussion of Sec. IV, it seems that the creation of an important flux of population to short distances is favored both by an important population cycling during the pulse and by a good transfer of this population back to the ground state. In other words, the optimal pulse should be as close as possible to a $(2n)\Pi$ pulse, with a negative chirp, and a large number n of cycles. This can be achieved with a pulse that is "following" the excited wave packet.

We have tentatively changed the parameters of the photoassociation pulse to check whether it is possible to optimize the compression effect. Starting from a transform limited pulse with the same spectral width as previously ($\delta\omega = 0.255\ \text{cm}^{-1}$, $\tau_L = 57.5$ ps) and with the same central frequency, the best results were obtained by increasing the linear chirp parameter χ and hence the temporal width. The optimal value was $\tau_C = 376.13$ ps, instead of 110 ps in the previous calculations. The duration of the pulse then becomes comparable with half the vibration period ($T_{\text{vib}}/2$) in the excited state. In order to make results comparable, the $\mathcal{E}_0$ factor in Eq. (8) was mutiplied by a factor compensating the variation of $\sqrt{\tau_L/\tau_C}$ factor in $f(t)$ in order to keep constant the maximum value of the coupling. The energy E_{pulse} is then multiplied by 6.25. The new pulse is closer to a $(2n)\Pi$ one, the number of Rabi oscillations reaches up to 24, the population transferred to the excited state has markedly decreased (3×10^{-4} instead of 2×10^{-3}).

The compression effect is now much more important, occurs earlier and is optimum at $t'_{\text{opt}} = t_P + 350$ ps. The wave packet at this time is displayed in Fig. 11, demonstrating a spectacular increase of the compression effect as compared to the previous results, and suggesting that the direction is the good one. The analysis of the results shows that the model of adiabatic transfer within a photoassociation window is still valid, but the impulsive approximation is no longer valid: New physical effects are present, which will be analyzed in a forthcoming paper [13].

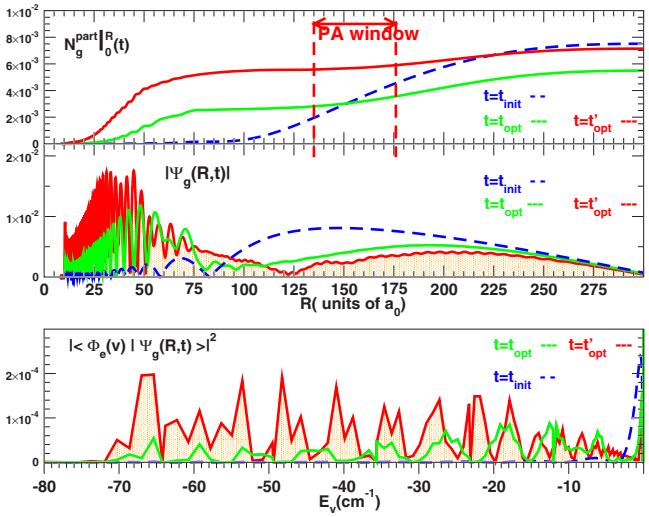

FIG. 11. (Color online) Improvement of the compression effect presented in Fig. 4, using the new pulse described in Sec. V, with a parameter τ_C comparable to the half vibration period in the excited state. Intermediate panel: Wave function $|\Psi_g(R,t=t_{\text{init}})|$ (broken blue line) of the initial collision state and ground state wave packet $|\Psi_g(R,t_{\text{opt}})|$ when the compression effect is maximum, after illuminating with the pulse $\mathcal{P}_-^{122}$ (green solid line, $t_{\text{opt}}=t_P+950$ ps) and the new pulse (red solid line, $t'_{\text{opt}}=t_P+350$ ps). Upper panel: integrated population $\int_0^R|\Psi_g(R',t)|^2dR'$, showing the increase of the probability density at short distances. Lower panel: Variation of the overlap $|\langle\Phi_e(v)|\Psi_g(R,t)\rangle|^2$ with the eigenfunctions for all the bound vibrational levels v in the $0_g^-(6S+6P_{3/2})$ excited potential curve, as a function of their binding energy E_v, for $t=t_{\text{init}}$ (broken blue line), $t=t_{\text{opt}}$ (green solid line), and $t=t'_{\text{opt}}$ (red solid line). The compressed wave packet is then better adapted for further photoassociation.

VI. CONCLUSION

The present paper was devoted to the analysis of the formation of a dynamical hole in the wave packet describing the relative motion of a pair of cold atoms in presence of a photoassociation pulse, and of the evolution of this wave packet after the pulse. As a case study, photoassociation of Cs into loosely bound levels of the outer well in $Cs_2 0_g^-(6S+6P_{3/2})$ was considered, using a pulse in the picosecond range, with a negative linear chirp parameter, designed in previous work [3,6] to create an excited wave packet with focussing properties. In the initial state, the wave packet is a stationary continuum wave function at the collision energy corresponding to 54 μK. Photoassociation with such a pulse can be interpreted as an adiabatic transfer of population within a photoassociation window, while the impulsive approximation is valid, since the motion of the nuclei can be neglected during the pulse. The numerical calculations show the creation of a dynamical hole in the region of the photoassociation window. The latter is created at distances where the ground-state potential and its gradient are negligible, while the excited state potential, with asymptotic R^{-3} behavior, has a significant gradient. The classical force is then supplying to the wave packet in the excited state an acceleration towards short distances.

After the pulse, the inner part of the ground-state wave packet is shown to move towards short distances, at a velocity typical of the vibrational motion in the excited state, due to the negative momentum kick gained from interaction with the laser field. This leads to a compression of population at short range, so that a second photoassociation pulse, red-detuned relative to the first one, and conveniently delayed, could be designed to bring much population to deeply bound levels of the excited state. Another signature of the dynamical hole is the redistribution of population in the ground state, with formation of pairs of hot atoms and population of the last bound level.

We have analyzed the momentum kick phenomenon by considering the time evolution of the local probability density and of the local current density. Spatially integrated values, giving the population and momentum on each channel, were considered, as well as partially integrated values, considering population below a certain distance. This procedure is necessary due to the delocalized character of the initial wave packet. The various terms included in the treatment have been discussed in the framework of a phase-amplitude formalism: In addition to the classical force and the force due to the coupling of the two channels by the laser, a third term has been pointed out.

The analysis for a pulse in the 100 ps range, widely used in previous work, with negative chirp, shows that, during the pulse duration, population and momentum exchange between the two channels occur due to Rabi cycling, so that the acceleration from the excited channel is transferred to the ground channel. After the pulse, the momentum gained by the inner part of the ground-state wave packet depends upon the number of Rabi cycles, upon the sign of the chirp (it is smaller in case of a positive chirp), and upon the amount of population transferred back to the ground state. It seems to be maximum for a pulse as close as possible to a $(2n)\Pi$ pulse, with which no photoassociated molecules are formed. In contrast, when considering a similar pulse with positive chirp, the photoassociation efficiency increases while the momentum kick is reduced.

Following these ideas, we have tentatively proposed photoassociation by a longer negatively chirped pulse, with duration similar to half the classical vibrational period in the excited state, so that the impulsive approximation is no longer valid. Such a pulse is designed to "follow" the motion of the excited wave packet during half the vibrational period. A strong increase of the momentum kick and of the compression effect in the ground state was indeed obtained, demonstrating that the direction is promising. Further analysis will be given in a forthcoming paper.

ACKNOWLEDGMENTS

This work has been supported by the European Union in the frame of the Cold Molecule EC network under Contract No. HPRN-CT-2002-00290. Ronnie Kosloff is grateful to Université Paris-Sud XI for a one month invitation as "professeur invité" to Laboratoire Aimé Cotton. The Fritz Haber Center is supported by the Minerva Gesellschaft für die Forschung GmbH München, Germany. Laboratoire Aimé Cotton is part of Fédération Lumière Matière (LUMAT, FR 2764).

[1] U. Banin, A. Bartana, S. Ruhman, and R. Kosloff, J. Chem. Phys. **101**, 8461 (1994).
[2] G. Ashkenazi, U. Banin, A. Bartana, R. Kosloff, and S. Ruhman, Adv. Chem. Phys. **100**, 229 (1997).
[3] E. Luc-Koenig, R. Kosloff, F. Masnou-Seeuws, and M. Vatasescu, Phys. Rev. A **70**, 033414 (2004).
[4] E. Luc-Koenig, M. Vatasescu, and F. Masnou-Seeuws, Eur. Phys. J. D **31**, 239 (2004).
[5] C. P. Koch, R. Kosloff, E. Luc-Koenig, F. Masnou-Seeuws, and A. Crubellier, J. Phys. B **39**, S1017 (2006).
[6] C. P. Koch, E. Luc-Koenig, and F. Masnou-Seeuws, Phys. Rev. A **73**, 033408 (2006).
[7] Albert Messiah, *Mecanique Quantique* (Dunod, Paris, 1960).
[8] Leonard I. Schiff, *Quantum Mechanics* (Mc Graw-Hill, New York, 1955).
[9] S. Kallush and R. Kosloff, Phys. Rev. A **76**, 053408 (2007).
[10] B. Brown and I. A. Walmsley, J. Phys. B **39**, S1055 (2006).
[11] M. J. Wright, J. A. Pechkis, J. L. Carini, S. Kallush, R. Kosloff, and P. L. Gould, Phys. Rev. A **75**, 051401 (2007).
[12] D. Bohm, Phys. Rev. **85**, 180 (1952).
[13] E. Luc-Koenig, F. Masnou-Seeuws, S. Kallush, and R. Kosloff (unpublished).